NACA TN 3706

NATIONAL ADVISORY COMMITTEE FOR AERONAUTICS

TECHNICAL NOTE 3706

INVESTIGATION OF THE LAMINAR AERODYNAMIC HEAT-TRANSFER CHARACTERISTICS OF A HEMISPHERE-CYLINDER IN THE LANGLEY 11-INCH HYPERSONIC TUNNEL AT A MACH NUMBER OF 6.8

By Davis H. Crawford and William D. McCauley

Langley Aeronautical Laboratory
Langley Field, Va.

Washington
July 1956

NATIONAL ADVISORY COMMITTEE FOR AERONAUTICS

TECHNICAL NOTE 3706

INVESTIGATION OF THE LAMINAR AERODYNAMIC HEAT-TRANSFER CHARACTERISTICS OF A HEMISPHERE-CYLINDER IN THE LANGLEY 11-INCH HYPERSONIC TUNNEL AT A MACH NUMBER OF 6.8

By Davis H. Crawford and William D. McCauley

SUMMARY

A program to investigate the aerodynamic heat transfer of a non-isothermal hemisphere-cylinder has been conducted in the Langley 11-inch hypersonic tunnel at a Mach number of 6.8 and a Reynolds number from approximately 1.09×10^5 to 1.03×10^6 based on diameter and free-stream conditions. The experimental heat-transfer coefficients were slightly less over the whole body than those predicted by the theory of Stine and Wanlass (NACA Technical Note 3344) for an isothermal surface. For stations within 45° of the stagnation point the heat-transfer coefficients could be correlated by a single relation between local Stanton number and local Reynolds number.

Pitot profiles taken at a Mach number of 6.8 on a hemisphere cylinder have verified that the local Mach number or velocity outside the boundary layer required in the theories may be computed from the surface pressures by using isentropic flow relations and conditions immediately behind a normal shock. The experimental pressure distribution at a Mach number of 6.8 is closely predicted by the modified Newtonian theory. The velocity gradients calculated by using modified Newtonian theory at the stagnation point vary with Mach number and are in good agreement with those obtained from measured pressures for Mach numbers from 1.2 to 6.8.

At the stagnation point, the theory of Sibulkin, using the diameter and conditions behind the normal shock, was in good agreement with the experiment when the velocity gradient at the stagnation point appropriate to the free-stream Mach number was used.

INTRODUCTION

One of the earliest experimental investigations in connection with heat transfer on a hemisphere-cylinder at supersonic speeds was carried

out by Eber (ref. 1) who obtained the "brake" temperature distribution along the surface. These brake or effective recovery temperatures decreased with increasing distance from the stagnation point on the hemisphere and were influenced by the free-stream Mach number. Korobkin (ref. 2) and Stine and Wanlass (ref. 3) show the same type of distributions and, in addition, demonstrate that for the hemisphere-cylinder with a laminar boundary layer the recovery factor η_r may be expressed by the square root of the Prandtl number based on the local conditions just outside the boundary layer.

Stalder and Nielsen (ref. 4) compared the average heat transfer (Nusselt number) with Reynolds number for different Mach numbers and found that, in their experiments, data at subsonic and low supersonic Mach numbers could be correlated when the supersonic data were based on conditions behind the normal shock. Experimental investigations of the local heat transfer on a hemisphere-cylinder have been made by Korobkin (refs. 2 and 5) and Stine and Wanlass (ref. 3). Stine and Wanlass noticed that, as the free-stream Mach number was increased, the pressure distributions were tending toward a common curve and suggested that the heat-transfer results they obtained at a Mach number of 1.97 could be representative of those obtained on similar isothermal surfaces with laminar boundary layer for Mach numbers greater than 1.97 and of temperatures less than that of dissociation. Although this tendency is correct, a Mach number of 1.97 is probably too low.

Some theoretical methods for obtaining local heat transfer on a hemisphere-cylinder at supersonic speeds have as their bases the solutions of incompressible flow on isothermal surfaces. An exact incompressible solution utilizing a method applied by Squire (presented in ref. 6) to a cylinder was given by Sibulkin in reference 7 for the heat transfer at the stagnation point. Sibulkin suggested that this solution may be applicable at supersonic speeds when conditions behind the normal shock are used. An approximate solution was derived for incompressible flow over a hemisphere with an isothermal surface by Sibulkin (presented in ref. 2) by assuming that the velocity and temperature profiles were similar and of parabolic shape. Korobkin (ref. 2) compared these theoretical results with his data at a Mach number of 2.80 and found that, when the incompressible-flow solution was adjusted so as to pass through Sibulkin's stagnation-point value, it roughly approximated the data. However, this result does not agree with the theory by Stine and Wanlass (ref. 3) who used a different approach. By using the Mangler transformation, the Stewartson transformation, and thermal solutions to the Falkner-Skan wedge-flow problem, they evaluated the heat-transfer rate in axisymmetric flow for an isothermal surface in terms of the known heat-transfer rate in an approximately equivalent two-dimensional flow.

The purpose of this investigation was to extend the range of the previous investigations for heat transfer on hemisphere-cylinders to a Mach number of 6.8. This investigation utilized data from transient

nonisothermal temperature distributions since, at the high temperature levels involved, an isothermal surface is difficult to obtain.

SYMBOLS

a	speed of sound
b	semihemispherical arc length
c_m	specific heat of model wall material
c_p	specific heat of air at constant pressure
c_v	specific heat of air at constant volume
D	diameter
h	local aerodynamic heat-transfer coefficient, $\frac{q}{T_r - T_s}$
k	thermal conductivity for air
k_m	thermal conductivity for model
L	a characteristic length
M	Mach number, u/a
Nu	Nusselt number, hL/k
Pr	Prandtl number, $c_p\mu/k$
p	pressure
q	heat flow to model per unit area, $-k\left(\frac{\partial T}{\partial y}\right)_s$
Re	Reynolds number, $\frac{\rho u L}{\mu}$
r	radius
St	Stanton number based on x and local free-stream conditions just outside boundary layer, $St = Nu/RePr = h/\rho u c_p$

T	absolute temperature
u	velocity
x	distance along body generator from stagnation point
y	space coordinate normal to body
z	distance along cylinder from juncture
β	velocity gradient along surface, $\frac{\partial u}{\partial x}$
ϵ	emissivity
η_r	recovery factor, $\frac{T_r - T_l}{T_t - T_l}$
θ	angle from stagnation point on sphere
μ	absolute viscosity
ν	kinematic viscosity
ξ	angle about axis of model
ρ	mass density of air
ρ_m	mass density of model shell material
σ	Stephen-Boltzmann constant
τ	time

Subscripts:

a	condition of model's surroundings
D	parameter based on static conditions immediately behind normal shock and with model diameter as a characteristic length
h	pitot tube behind bow shock
i	not corrected for heat conduction along model skin
in	local condition on inside surface of model shell
L	parameter using L as characteristic length
r	recovery, surface temperature

s	local conditions on outside surface of model
t	stagnation conditions
x	parameter based on static conditions just outside boundary layer and with x as characteristic length
σ	static conditions immediately behind normal shock
l	local conditions just outside boundary layer
∞	undisturbed free-stream conditions

APPARATUS

Tunnel

The present investigation was conducted in the Langley 11-inch hypersonic tunnel described in references 8 and 9. Air is stored at 50 atmospheres pressure and is released through an adjustable pressure regulating valve and a new direct air heater with tube resistance elements of nickel-chromium alloy (replacing the storage heater described in refs. 8 and 9) to the settling chamber and nozzle. A two-dimensional nozzle constructed of Invar and designed for a Mach number of 7 was used for this investigation. Invar was used in the construction of this nozzle in order to alleviate the deflection of the first minimum, which occurred in the steel nozzle because of differential heating of the nozzle blocks. Preliminary calibrations have indicated a Mach number of 6.86 ± 0.04 at 30 atmospheres stagnation pressure in the central core of uniform flow which measures about $6\frac{1}{2}$ inches in the vertical direction by about 6 inches in the horizontal direction.

Tunnel Conditions

During the tests the tunnel was operated through a stagnation-temperature range from $1,040^\circ$ R to $1,160^\circ$ R and through a stagnation-pressure range from 10 to 31 atmospheres. The free-stream Reynolds numbers (based on body diameter) were in the range from approximately 3.4×10^5 to 1.03×10^6. The calibrated tunnel Mach number at the model nose was used to correlate the data. In these tests, the model nose was approximately 6 inches ahead of the center of the test section. At this point, the tunnel calibration gives a Mach number of 6.82 for a stagnation pressure of 31 atmospheres, which agrees with values obtained from pressures at the nose of the pressure model. As the pressure decreases,

the Mach number also decreases slightly, so that, at 10 atmospheres stagnation pressure, the Mach number 6 inches ahead of the test-section center line is 6.74.

Instrumentation

The temperature measurements included stagnation temperature and model skin temperature. The stagnation temperature was measured by shielded thermocouples distributed at various stations in the settling chamber.

The potentiometers used for recording the model temperature showing greatest transient rate of change were cyclic printers with a 1-second interval, and with a 1-second full-scale response. In order to reduce uncertainties associated with the time response of the recording instruments, the thermocouples on the sphere were connected to be read in order of decreasing temperature about the sphere from station 1 to station 11. The temperature at station 1 was recorded twice to allow time for balancing out the large temperature change between stations 1 and 11. Four instruments were connected to read the temperatures of the first 11 thermocouples in this manner and were synchronized so that each thermocouple was read once each 3 seconds by one of the potentiometers.

Model surface pressures were recorded on film by the evacuated capsule instruments described in reference 8. The motion of a diaphragm rotates a small mirror to displace the trace of a light beam falling on a moving film. Pressure cells were chosen to give as near full-scale deflection as possible for the measuring station. The stagnation pressure was measured with high-accuracy Bourdon tube gages.

Schlieren System

Two schlieren systems were used in this investigation. One system had a single-pass, vertical Z-light path with a horizontal knife edge, and the other, a double-pass horizontal light path with the light source and cut-off knife edge at the center of curvature of the concave spherical mirror. The double-pass system was used only when greater sensitivity was needed for boundary-layer study. Film exposures were of approximately 3 microseconds duration.

Models

The four models used in this investigation are shown in figures 1 and 2. The pressure-distribution and heat-transfer models were constructed of SAE 1020 carbon steel and the temperature-recovery model was constructed

by electroplating nickel on a mandrel. The dimensions of the heat-transfer models were carefully measured before the parts were assembled with silver solder.

The large temperature-distribution model was 3.025 inches in diameter, 10.5 inches in length, and varied from 0.098 inch to 0.101 inch in wall thickness. It contained 25 thermocouples, silver soldered into holes in the model skin so that their effective measuring junctions were located on the inner surface. These thermocouples were of No. 36 gage chromel alumel wire and were arranged in a spiral of one revolution on the hemisphere and of two revolutions on the cylinder. Ten of these thermocouples were located on the hemisphere, fourteen were on the cylinder, and one was on the sphere-cylinder juncture as given in figure 1.

The pressure-distribution model was 3.000 inches in diameter, 10.5 inches in length, and 0.10 inch in wall thickness and contained 16 pressure orifices located as shown in figure 1. Two of the orifices were located on the base of the model. The orifices were 0.040 inch in diameter and were arranged in a spiral of one revolution about the sphere in order to reduce any orifice-interference effect. The orifices on the cylinder were also arranged in a spiral of one revolution.

The small temperature-distribution model was 1.170 inches in diameter, 5.32 inches in length, and varied from 0.030 inch to 0.035 inch in wall thickness. Temperature measurements on this model were taken from eight chromel alumel thermocouples of No. 30 gage wire, five of these being located at stations from the stagnation point to the sphere-cylinder juncture.

The temperature-recovery model constructed of electroplated nickel was 2.000 inches in diameter, 5.00 inches in length, and 0.005 inch thick. Temperature measurements were taken from 14 chromel alumel thermocouples of No. 30 gage wire.

ANALYSIS

Heat Transfer to Model

The local rate of heat flow into the model was calculated from the local temperatures as a function of time and position. The general heat-conduction equation (ref. 10) in a homogeneous material is

$$\frac{\partial T}{\partial \tau} = \frac{k_m}{\rho_m c_m} \nabla^2 T \qquad (1)$$

In spherical coordinates this equation becomes:

$$\frac{\partial T}{\partial \tau} = \frac{k_m}{\rho_m c_m}\left[\frac{1}{r^2}\frac{\partial}{\partial r}\left(r^2\frac{\partial T}{\partial r}\right) + \frac{1}{r^2 \sin\theta}\frac{\partial}{\partial \theta}\left(\sin\theta\frac{\partial T}{\partial \theta}\right) + \frac{1}{r^2 \sin\theta}\frac{\partial^2 T}{\partial \xi^2}\right] \qquad (2)$$

Since the model shell is relatively thin with respect to its other dimensions, it is assumed that the first and second derivatives of T with respect to θ and ξ, as well as the first derivative of T with respect to τ, are independent of r. Equation (2) may then be integrated once with respect to r, using the boundary condition $\frac{\partial T}{\partial r} = 0$ at the inner surface where $r = r_{in}$, and then may be solved for $\frac{\partial T}{\partial r}$ to obtain the following:

$$\frac{\partial T}{\partial r} = \left(\frac{r^3 - r_{in}^3}{3r^2}\right)\frac{\rho_m c_m}{k_m}\frac{\partial T}{\partial \tau} - \left(\frac{r - r_{in}}{r^2 \sin\theta}\right)\frac{\partial}{\partial \theta}\left(\sin\theta\frac{\partial T}{\partial \theta}\right) - \left(\frac{r - r_{in}}{r^2 \sin\theta}\right)\frac{\partial^2 T}{\partial \xi^2} \qquad (3)$$

Equation (3) may then be evaluated at the outer surface where $r = r_s$ and at zero angle of attack so that T is independent of ξ; this evaluation gives the following:

$$\left(\frac{\partial T}{\partial r}\right)_s = \left(\frac{r_s^3 - r_{in}^3}{3r_s^2}\right)\frac{\rho_m c_m}{k_m}\frac{\partial T}{\partial \tau} - \left(\frac{r_s - r_{in}}{r_s^2 \sin\theta}\right)\frac{\partial}{\partial \theta}\left(\sin\theta\frac{\partial T}{\partial \theta}\right) \qquad (4)$$

However at the surface,

$$q_s = -k_m\left(\frac{\partial T}{\partial r}\right)_s \qquad (5)$$

Therefore,

$$q_s = -\rho_m c_m\left(\frac{r_s^3 - r_{in}^3}{3r_s^2}\right)\frac{\partial T}{\partial \tau} + k_m\left(\frac{r_s - r_{in}}{r_s^2 \sin\theta}\right)\frac{\partial}{\partial \theta}\left(\sin\theta\frac{\partial T}{\partial \theta}\right) \qquad (6)$$

An examination of the above equation discloses that the first term on the right represents q_i, the local net heat storage which would be

realized in a shell element if the conduction were zero. The term $\left(\frac{r_s^3 - r_{in}^3}{3r_s^2}\right)$ is approximately $(r_s - r_{in})$, or the shell thickness, so that in the limit as $t \rightarrow 0$, the q_i term becomes the same as that used for a flat plate. The second term on the right represents the local net heat conducted along the model shell.

When this equation was used to calculate q_s at the various times and stations, the values of $\frac{\partial T}{\partial \tau}$ for the heat-storage term were taken from faired curves of temperature plotted against time. The values of $\frac{\partial}{\partial \theta}\left(\sin \theta \frac{\partial T}{\partial \theta}\right)$ for the conduction term were found graphically by taking slopes of faired curves.

In order to give a comparison of the relative size of the heat-storage and conduction terms for the tests using the 3.025-inch-diameter heat-transfer model, typical q_s and q_i values are plotted in figure 3 for a time early in the run and for a time late in the run. The difference between these curves $q_s - q_i$ is the value of the conduction term. It is seen that, at 5 seconds from the start of the run, the conduction term is only 20 percent of q_s for the station at the stagnation point; but, near the end of the run, the conduction term is about 70 percent of q_s at the same station.

The local heat-transfer coefficients were determined from the standard heat-flow equation for convection, $q_s = h(T_s - T_r)$. The quantities T_r and h were assumed constant for a given set of test conditions, and h was determined from the slope of the straight-line variation of q_s plotted against T_s as is shown in figure 4. In the present tests, there were some variations in the test conditions during a run. The stagnation temperature sometimes varied 20°, and the pressure varied nearly 5 percent in the lowest pressure run. In order to correct partially for the variation in stagnation temperature, the values of q_s/T_t were faired through a calculated value of T_r/T_t. The recovery temperature ratios used in the fairing for the determination of h were obtained from the recovery factors for a flat plate given by Van Driest (ref. 11) by using the local flow conditions at the outside edge of the boundary layer.

Errors

The present heat-transfer tests were affected by four small sources of error which were of uncertain magnitude and were not directly

incorporated in the computations. One source was the heat loss from the model by radiation, and another was the heat loss by conduction down the thermocouple wire. The third was the assumption that the difference in temperature distribution between the outside and the inside surfaces of the model was negligible. The fourth source of error is the assumption that the heat-transfer coefficient is independent of the temperature level. The error associated with radiation was estimated to be about 3 percent of the value of q at the highest temperature condition. The error associated with heat flow down the thermocouple wire was not estimated directly but was assumed to be small, especially on the large heat-transfer model where the thickness of the model was 0.10 inch and the diameter of the thermocouple wire was 0.005 inch. The temperature difference between the outside and the inside skin surface was less than 10° F at the stagnation point immediately after the start of a run at $p_t = 31$ atmospheres. This temperature difference represented an error of less than 0.01 in the determination of T_s/T_t. It was noticed, however, that each of the first three errors tended to reduce the calculated value of the heat-transfer coefficient, so that the final results of this data analysis might tend to be slightly low when compared with theory. For the assumption that the heat-transfer coefficient is independent of the temperature level, the maximum variation in wall temperature occurred at the stagnation point and here the wall temperature varied from 180° F to 550° F. By the theory of Reshotko and Cohen (ref. 12) a variation in wall temperature of this magnitude would result in a deviation of only $\pm 1\frac{1}{2}$ percent from the mean value of $Nu/\sqrt{Re}$ at the stagnation point.

RESULTS AND DISCUSSION

Pressure Distribution

The longitudinal pressure distributions for the hemisphere-cylinder at zero lift are presented in figure 5 for Reynolds numbers of 0.71×10^5 and 1.42×10^6 based on diameter and conditions behind the normal shock. These pressure distributions are presented as a ratio of local pressure coefficient to the pressure coefficient at the stagnation point. This pressure distribution has been compared with the Newtonian theory from reference 13, the data of Stine and Wanlass (ref. 3) at $M = 1.97$ and 3.80, and the data of Oliver (ref. 14) at $M = 5.8$. It will be noted that, at Mach numbers above 3.80, the pressure-coefficient distribution curves asymptotically approach a single curve, and the local Mach number distribution on the hemisphere becomes independent of the free-stream Mach number. This was pointed out in reference 3 and is in accordance with the hypersonic similarity parameter (ref. 15) which predicts that the flow pattern about an arbitrary body will become stationary as Mach number increases; for a blunt body, this tendency occurs at a lower Mach number than that for a slender body.

In this report, the isentropic-flow relations between the pressures measured at the stagnation point and the local surface pressures measured at subsequent stations were used to calculate local flow conditions just outside the boundary layer. The validity of this method was investigated by the use of pitot surveys of the boundary layer. In figure 6, the pitot profiles are presented for the hemisphere-cylinder juncture, a station midway along the cylinder, and a station 1/8 inch in front of the base of the cylinder. These profiles are characteristic of laminar profiles and indicate that the boundary layer remains laminar over the whole body. The point where the pitot profiles break away from the characteristic boundary-layer profile corresponds closely to the pitot ratio obtained by using the static surface pressure from the pressure model and the isentropic-flow relations (ref. 16) from the stagnation point to the survey stations. Thus, the pressures from the body surfaces are sufficient through the use of isentropic-flow relations to obtain local flow conditions outside the boundary layer for station at least up to $\frac{x}{b} = 4.8$. In figures 7 and 8, the local Mach number and temperature ratio are presented as computed in this manner. It will be noted that the curves exhibit a slight change for different Reynolds number which was due to a change in calibrated tunnel Mach number at different pressure levels.

Laminar Recovery Factor

The calculated values of the ratio T_r/T_t and of the laminar recovery factor are shown in figure 9. The recovery factors were calculated by a method of Van Driest (ref. 11) and by $\eta_r = \sqrt{Pr_l}$. These values are compared with data from the recovery-temperature model. Included are the recovery temperature ratios and the recovery factors calculated from the uncorrected recovery temperatures or equilibrium temperatures, and also from the recovery temperatures corrected for conduction and radiation.

The laminar recovery factor was also calculated from $\eta_r = \sqrt{Pr}$, where the Prandtl number was calculated for the average of the total and the local stream temperature as was suggested by Stine and Wanlass (ref. 3). The results of this calculation agreed closely with those from the method of Van Driest and were not included in figure 9.

The experimental values of T_r/T_t were corrected for conduction and radiation by first calculating the local heat flow into the model at equilibrium temperature and then by using this value of q_s to obtain a value of q_s/T_t to plot on the respective curves of q_s/T_t against T/T_t. In

this way a point was obtained sufficiently near the T/T_t axis to enable the fairing from the heat-transfer-model data to $q_s/T_t = 0$. The value of T_r/T_t obtained by this method was the recovery temperature corrected for radiation and conduction.

The local heat flow q_s into the model at equilibrium temperatures was calculated by using the following equation:

$$q_s = k\left(\frac{r_s - r_{in}}{r^2 \sin\theta}\right)\frac{\partial}{\partial\theta}\left(\sin\theta\,\frac{\partial T}{\partial\theta}\right) + \sigma\epsilon\left(T_s^4 - T_a^4\right) \tag{7}$$

The first term on the right represents the heat flow into the model as found by equation (6) for a model in equilibrium, that is, $\frac{\partial T}{\partial \tau} = 0$. The second term on the right represents the heat flow into the model which is lost by radiation. In a slightly different notation this relation is shown in reference 17. The temperature of the surroundings T_a was assumed to be constant at 140° F over the entire hemisphere.

In order to apply equation 7, an estimate of the emissivity must be made. This estimate depends upon the surface condition of the material as well as the kind of material and its temperature. At the start of the testing the model had a polished surface, but after the testing the surface of the hemisphere had become slightly roughened. This roughness was greatest at the stagnation point and was slight at the sphere-cylinder juncture. Because of the uncertainty in the value of the emissivity at the elevated temperatures of these tests, it was assumed to be constant (0.15) over all the model. It was felt that this estimated value of emissivity was not in error by more than ±0.05.

When the corrected values of temperature ratio T_r/T_o are compared with the values obtained from the two theories, the experimental data does not decisively select either theory. Since the Van Driest method considers a local Mach number effect on the recovery temperature ratio, the values of T_r/T_o obtained by the method were used in the reduction of the heat-transfer data.

Temperature Distribution

Surface-temperature distributions obtained for various times during a typical run on the heat-transfer model are presented in figure 10. At the nose the average value of the temperature was about 700° R and on the cylinder about 600° R giving values of T_s/T_∞ of approximately 7 and 6, respectively.

Heat-Transfer Parameters $Nu/\sqrt{Re}$

The local laminar heat-transfer parameter was calculated on the basis of two different characteristic lengths. For one parameter $Nu_x/\sqrt{Re_x}$, the characteristic length was the distance x along the body generator from the stagnation point. The air-flow properties used in this parameter were the local flow conditions just outside the boundary layer. The values of this parameter for $M = 6.8$ are shown in figure 11 along with the range of experimental data at $M = 1.97$ from reference 3. These experimental values are compared with theories by Stine and Wanlass (ref. 3), by Chapman and Rubesin (ref. 18), with a modification of a theory by Sibulkin (ref. 7), and with a theory by Reshotko and Cohen (ref. 12). For the other heat-transfer parameter $Nu_D/\sqrt{Re_D}$ the diameter of the model was used as the characteristic length, and the air-flow properties used were taken as those immediately behind the normal shock in the center of the bow wave. The values of this parameter for $M = 6.8$ as well as the range of values for $M = 1.97$ (ref. 3) are shown in figure 12. These values are compared with the theory by Stine and Wanlass and with a second modification of the theory by Sibulkin.

The local heat-transfer parameter $Nu_x/\sqrt{Re_x}$, as calculated by the theory of Stine and Wanlass, is based upon the local Mach number distribution at the outer edge of the boundary layer and upon the local Prandtl number. In the present tests, the Prandtl number varied from about 0.68 at the stagnation point to about 0.74 near the end of the cylinder. A value of $Pr = 0.70$ was used throughout the calculation of the theory of Stine and Wanlass. This caused an estimated maximum deviation from the mean heat-transfer parameter of only 2 percent.

In the Stine and Wanlass theory, the assumption is made that the difference between the actual wall temperature and the insulated wall temperature is small. In the present tests, this temperature difference varied from about 100° F to about 500° F. An examination of figure 11 discloses that the data points have a tendency to fall below the theory. This difference may be due in part to the rather large temperature difference. The reasonable agreement of the data with the theory, however, shows that the theory of Stine and Wanlass may be used with good results even when the insulated wall temperature and the actual wall temperature are quite different.

In comparing the theoretical results of Stine and Wanlass at $M = 6.8$ and at $M = 1.97$, a slight discrepancy appears in that a discontinuity occurred at the hemisphere-cylinder juncture ($x/b = 1.00$) for $M = 6.8$ and not at $M = 1.97$. This discontinuity can be traced to a difference in local Mach number distributions obtained from the two investigations. In this investigation, the pressure distribution has an abrupt change in slope at the juncture (from a high pressure gradient to a very low pressure gradient) which gives a similar change in the local Mach number gradient (fig. 7). In reference 3, no such change was noted in the

pressure distribution, and thus the local Mach number gradient had a gradual change at the juncture resulting in a continuous curve for the local heat-transfer parameter based on x. Theoretically, a discontinuous pressure gradient is predicted at the juncture.

Although the use of the theory of Stine and Wanlass leads to the calculation of the local heat-transfer parameter $Nu_x/\sqrt{Re_x}$, the parameter $Nu_D/\sqrt{Re_D}$ may be calculated from the parameter based on x, when the free-stream Mach number, the local Mach number on the model, and the stagnation temperature are known. When the experimental and theoretical values of the parameter $Nu_x/\sqrt{Re_x}$ in reference 3 were converted to $Nu_D/\sqrt{Re_D}$, a stagnation temperature of 520° R was assumed.

The theory of Chapman and Rubesin (ref. 18) is a method of obtaining the values of the local heat-transfer parameter for a flat plate. The air-flow properties used were those at the outer edge of the boundary layer. The distance along the body generator was taken as the flat-plate distance from the leading edge. This theory depends directly upon the air temperature at the outer edge of the boundary layer and upon the surface temperature and is not directly a function of the Mach number. The theory evaluation at $M = 1.97$ is that shown in reference 3.

In reference 7, Sibulkin suggested applying his incompressible solution for stations near the stagnation point of a sphere to the nose of a blunt body moving at supersonic speeds by using as free-stream conditions those behind the center of the bow wave. Since the velocity gradient at the nose would not be expected to be the same as in incompressible flow, Sibulkin's equation should be used before the incompressible velocity gradient around the sphere is incorporated, which gives

$$Nu_L = 0.763Pr^{0.4}{}_L\left(\frac{\beta}{\nu}\right)^{0.5} \tag{8}$$

The relation was derived with the assumption of incompressible flow, but the author suggests that the theory may be valid for the flow near the stagnation point of a blunt body in a supersonic stream.

Equation (8) may be written as

$$\frac{Nu_L}{\sqrt{Re_L}} = \frac{\frac{hL}{k}}{\sqrt{\frac{\rho u L}{\mu}}} = 0.763Pr^{0.4}\left(\frac{\beta L}{u}\right)^{0.5} \tag{9}$$

When the characteristic length is x and the flow velocity and other physical conditions of the air are evaluated at the outer edge of the boundary layer, the first modification of Sibulkin's theory is obtained. This appears as follows:

$$\frac{Nu_x}{\sqrt{Re_x}} = \frac{\frac{hx}{k_1}}{\sqrt{\frac{\rho u x}{\mu}}}$$

$$= 0.763Pr^{0.4} \tag{10}$$

The theoretical heat-transfer parameter evaluated in this manner is a function only of the Prandtl number.

When the characteristic length is D and the flow velocity and other physical properties of the air are evaluated immediately behind the normal shock, equation (9) becomes

$$\frac{Nu_D}{\sqrt{Re_D}} = \frac{\frac{hD}{k_\sigma}}{\sqrt{\frac{\rho_\sigma \mu_\sigma D}{\mu_\sigma}}}$$

$$= 0.763Pr^{0.4}\left(\frac{\beta D}{u_\sigma}\right)^{0.5} \tag{11}$$

This equation is the second modification of Sibulkin's theory used in this report. The theoretical heat-transfer parameter evaluated in this manner is a function of the Prandtl number and of $\frac{\beta D}{u_\sigma}$.

In figure 13(a), the values of u_1/u_σ are plotted against x/D on the hemisphere. These curves show that β is constant near the stagnation point at a given Mach number. In figure 13(b), experimental values of $\beta D/u_\sigma$ from several references, as well as curves computed by using modified Newtonian and incompressible flow theories, are plotted against Mach number. This curve shows that $\beta D/u_\sigma$ is a function of Mach number. Therefore, $Nu_D/\sqrt{Re_D}$, as found by Sibulkin's theory near the stagnation point, is a function of Mach number.

When the Newtonian theory was used to find $\beta D/u_\sigma$, the Newtonian pressure coefficient as shown in figure 5 was used to determine the pressure distribution around the nose of the hemisphere. The correct pressure coefficient at the stagnation point to be used with each Mach number was found from normal-shock-flow relations (ref. 16). The isentropic-flow relations between the pressure at the stagnation point and the surface pressures computed for subsequent stations were used to calculate the local flow conditions just outside the boundary layer. This is the same procedure that was used to calculate the local flow conditions from the measured pressures.

In figure 11 it is seen that the data indicates a value at the stagnation point about 10 percent below the value of $Nu_x/\sqrt{Re_x}$ as found by Sibulkin's method. In this figure it is seen that the data from tests at two different Mach numbers, $M = 1.97$ and $M = 6.8$, agree within the scatter of the data. In figure 12, it is seen that the data at the free-stream Mach numbers of 1.97 and 6.8 indicate values which, within the scatter, are consistent with the predictions of $Nu_D/\sqrt{Re_D}$ by Sibulkin's method. It is important to note, however, that the variation of $\beta D/u_\sigma$ with the free-stream Mach number must be taken into account and that the prediction of β by the potential theory may not be used for a hemispherical nose subjected to supersonic flow.

Local Stanton Number

In figure 14 the local Stanton number is plotted against the local Reynolds number. The data presented includes points from $\theta = 5^\circ$ to $\theta = 45^\circ$ on the hemisphere surface.

By assuming that the velocity and temperature boundary-layer profiles were similar and of parabolic shape, Sibulkin (presented in ref. 2) derived an approximate solution for Nu_D over the entire hemisphere for incompressible flow which, when transformed for the local conditions outside the boundary layer and distance from the stagnation point, becomes

$$Nu = k(\theta)x\left(\frac{\beta}{\nu}\right)^{0.5}Pr^{0.4} \tag{12}$$

where $k(\theta)$ is a proportionality function which depends on the angular position of the point under consideration measured from the axis of flow symmetry.

If β is assumed constant (a valid assumption for θ up to 45° in these tests, see fig. 13), the equation reduces to

$$Nu = k(\theta)Re^{0.5}Pr^{0.4} \tag{13}$$

From reference 6 it may be seen that $k(\theta)$ may be approximated near the stagnation point by the value of 0.763, and the local Stanton number near the stagnation point becomes

$$St = \frac{Nu}{RePr}$$

$$= 0.763Re^{-0.5}Pr^{-0.6} \tag{14}$$

For this equation to give the correct Stanton number around the hemisphere surface, du/dx or β must be constant and $k(\theta)$ should not depart radically from the value of 0.763.

In figure 14 the heat-transfer data has been compared with Sibulkin's stagnation-point solution shown in equation (14). As seen from figure 13(a), β can be considered constant up to values of θ greater than 45° $\left(\frac{x}{D} = 0.4\right)$. In figure 11 an indication of the variation of $k(\theta)$ may be obtained from the decrease of the heat-transfer parameter from the constant stagnation-point value as x is increased. Indeed, even the difference in level which is observed between the stagnation-point curve and the data in figure 14 may also be detected in figure 11. Sibulkin's stagnation-point value is approximately 9 percent above the data at the nose and about 15 percent above the data at the 45° station. Above 45°, $k(\theta)$ diverges rapidly and β begins to diverge. Inasmuch as the data above 45° do not correlate, they are not presented in figure 14.

Average Heat-Transfer Coefficient

The average heat-transfer coefficient determined experimentally in this investigation and by Stalder and Nielsen in reference 4 are presented in figure 15. The data from Stalder and Nielsen are those for $M = 0.12$ to 0.17, $M = 1.75$, and $M = 2.67$. Also included in figure 15 are experimental points found by an integration of experimental data by Stine and Wanlass (ref. 3) at $M = 1.97$. The data has been compared with values found by using the theory of Stine and Wanlass at $M = 1.97$ and $M = 6.8$ and with the incompressible theory of Sibulkin used by Korobkin (ref. 2). Korobkin adjusted the latter solution to pass through the stagnation point for incompressible flow (ref. 7).

The data from Stalder and Nielsen (ref. 4) for Mach numbers below 2.67 appear to correlate with the adjusted incompressible theory. The data of reference 4 were evaluated, however, in a different manner from the data of this paper. In the present paper the local values of the heat-transfer coefficient were calculated from the local heat convection and the local recovery temperature. Then these local values of h were integrated over the area of the hemisphere to find the average value. In reference 4 the average heat-transfer coefficients were evaluated by measuring the total heat convection to the hemisphere and an "effective" average recovery temperature found by an extrapolation to zero net heat transfer to the surface. The different results as found by the two methods are seen in figure 15.

The integrated data from Stine and Wanlass and the data from this investigation show a good correlation at Mach numbers of 1.97 and 6.80 and Reynolds numbers from 0.002×10^6 to 2.28×10^6.

Schlieren Observations

The normal shock and body boundary layer are shown in the schlieren photographs (fig. 16) for a single-pass and double-pass schlieren system. The relatively nonsensitive single-pass system clearly shows the normal shock while the sensitive double-pass system was used to show that the boundary layer is laminar on the surface of the cylinder. The two flow photographs appear to show additional disturbances about three-fifths of the distance along the cylinder from the hemisphere-cylinder juncture. These disturbances result from the intersection of the bow shock wave and the boundary layer at the windows. The heating effect was great enough so that a similar picture of this region was obtained immediately after a run, as shown in the post-run zero picture for the double-pass system.

CONCLUSIONS

A program to investigate the aerodynamic heat transfer of a nonisothermal hemisphere-cylinder has been conducted in the Langley 11-inch hypersonic tunnel at a Mach number of 6.8 and a Reynolds number from approximately 1.09×10^5 to 1.03×10^6 based on diameter and free-stream conditions. In this investigation the boundary layer was laminar having average values of T_s/T_∞ at the nose of about 7 and about 6 on the cylinder (where T_s is the local free-stream temperature just outside the boundary layer and T_∞ is the free-stream temperature ahead of the normal shock). The data have been correlated with theoretical analyses and results of other experiments at lower Mach numbers. The following results were obtained:

1. The experimental heat-transfer coefficients from this investigation on a nonisothermal (constant wall thickness) hemisphere-cylinder with heat flowing to the surface were slightly less over the whole body than those predicted by the theory of Stine and Wanlass (NACA Technical Note 3344) for an isothermal surface.

2. A modification of Sibulkin's stagnation point solution gave the trend of the local Stanton number with local Reynolds number for angles up to 45° from the stagnation point. The calculated values, however, were approximately 12 percent higher than the experimental values.

3. Pitot profiles taken at a Mach number of 6.8 on a hemisphere-cylinder have verified that the local Mach number or velocity outside the boundary layer required in the use of the theories may be computed from the surface pressures by using isentropic flow relations and conditions behind a normal shock. The experimental pressure distribution at a Mach number of 6.8 is closely predicted by the modified Newtonian theory. The velocity gradients calculated by using modified Newtonian theory at the stagnation point vary with Mach number and are in good agreement with those obtained from measured pressures for Mach numbers from 1.2 to 6.8.

4. At the stagnation point, a second modification of the theory by Sibulkin using the diameter and conditions behind the normal shock was in good agreement with the experiment when the velocity gradient at the stagnation point appropriate to the free-stream Mach number was used.

Langley Aeronautical Laboratory,
National Advisory Committee for Aeronautics,
Langley Field, Va., March 21, 1956

REFERENCES

1. Eber, G. R.: Recent Investigation of Temperature Recovery and Heat Transmission on Cones and Cylinders in Axial Flow in the N.O.L. Aeroballistics Wind Tunnel. Jour. Aero. Sci., vol. 19, no. 1, Jan. 1952, pp. 1-6, 14.

2. Korobkin, Irving: Local Flow Conditions, Recovery Factors and Heat-Transfer Coefficients on the Nose of a Hemisphere-Cylinder at a Mach Number of 2.8. NAVORD Rep. 2865 (Aeroballistic Res. Rep. 175), U. S. Naval Ord. Lab. (White Oak, Md.), May 5, 1953.

3. Stine, Howard A., and Wanlass, Kent: Theoretical and Experimental Investigation of Aerodynamic-Heating and Isothermal Heat-Transfer Parameters on a Hemispherical Nose With Laminar Boundary Layer at Supersonic Mach Numbers. NACA TN 3344, 1954.

4. Stalder, Jackson R., and Nielsen, Helmer V.: Heat Transfer From a Hemisphere-Cylinder Equipped With Flow-Separation Spikes. NACA TN 3287, 1954.

5. Korobkin, Irving: Laminar Heat Transfer Characteristics of a Hemisphere for the Mach Number Range 1.9 to 4.9. NAVORD Rep. 3841 (Aeroballistic Res. Rep. 257), U. S. Naval Ord. Lab. (White Oak, Md.), Oct. 10, 1954.

6. Fluid Motion Panel of the Aeronautical Research Committee and Others: Modern Developments in Fluid Dynamics. Vol. II, ch. XIV, sec. 270, S. Goldstein, ed., The Clarendon Press (Oxford), 1938.

7. Sibulkin, M.: Heat Transfer Near the Forward Stagnation Point of a Body of Revolution. Jour. Aero. Sci. (Readers' Forum), vol. 19, no. 8, Aug. 1952, pp. 570-571.

8. McLellan, Charles H., Williams, Thomas W., and Bertram, Mitchel H.: Investigation of a Two-Step Nozzle in the Langley 11-Inch Hypersonic Tunnel. NACA TN 2171, 1950.

9. McLellan, Charles H., Williams, Thomas W., and Beckwith, Ivan E.: Investigation of the Flow Through a Single-Stage Two-Dimensional Nozzle in the Langley 11-Inch Hypersonic Tunnel. NACA TN 2223, 1950.

10. Wylie, C. R., Jr.: Advanced Engineering Mathematics. McGraw-Hill Book Co., Inc., 1951, pp. 206-208.

11. Van Driest, E. R.: The Laminar Boundary Layer With Variable Fluid Properties. Rep. No. AL-1866, North American Aviation, Inc., Jan. 19, 1954.

12. Reshotko, Eli, and Cohen, Clarence B.: Heat Transfer at the Forward Stagnation Point of Blunt Bodies. NACA TN 3513, 1955.

13. Grimminger, G., Williams, E. P., and Young, G. B. W.: Lift on Inclined Bodies of Revolution in Hypersonic Flow. Jour. Aero. Sci., vol. 17, no. 11, Nov. 1950, pp. 675-690.

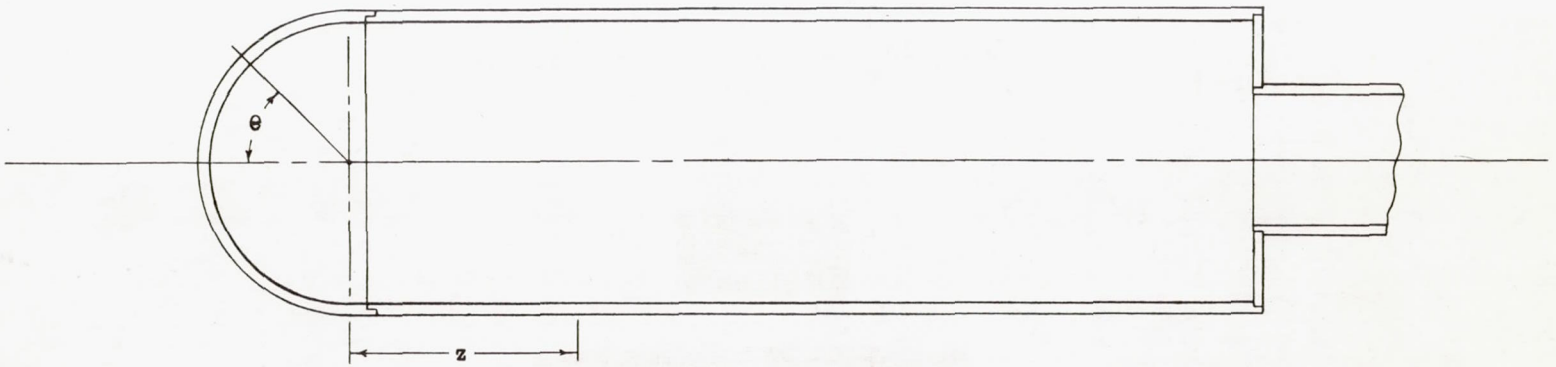
14. Oliver, Robert E.: An Experimental Investigation of Flow Over Simple Blunt Bodies at a Nominal Mach Number of 5.8. GALCIT Memo. No. 26 (Contract No. DA-04-495-Ord-19), June 1, 1955.

15. Tsien, Hsue-shen: Similarity Laws of Hypersonic Flows. Jour. Math. and Phys., vol. XXV, no. 3, Oct. 1946, pp. 247-251.

16. Burcher, Marie A.: Compressible Flow Tables for Air. NACA TN 1592, 1948.

17. McAdams, William H.: Heat Transmission. Second ed., McGraw-Hill Book Co., Inc., 1942, pp. 52 and 394.

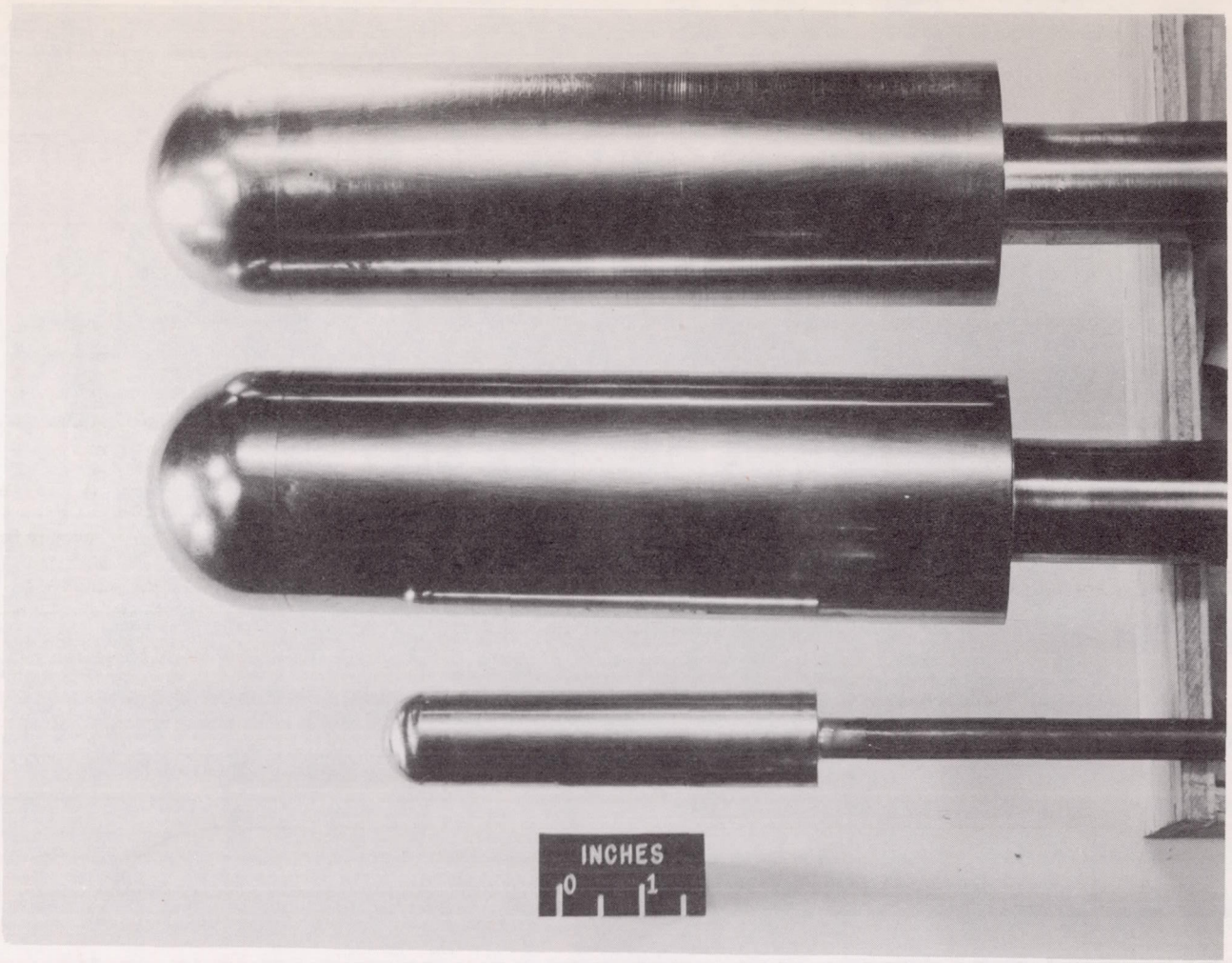
18. Chapman, Dean R., and Rubesin, Morris W.: Temperature and Velocity Profiles in the Compressible Laminar Boundary Layer With Arbitrary Distribution of Surface Temperature. Jour. Aero. Sci., vol. 16, no. 9, Sept. 1949, pp. 547-565.



Orifice and Thermocouple Locations

Pressure Model 3.000" O. D.				Heat Transfer Model 1.170" O. D.				Heat Transfer Model 3.025" O. D.				Recovery Temperature Model 2.000" O. D.			
Hemisphere		Cylinder		Hemisphere		Cylinder		Hemisphere		Cylinder		Hemisphere		Cylinder	
Station	θ	Station	z	Station	θ	Station	z	Station	θ	Station	z	Station	θ	Station	z
1	0°	8	.393"	1	0°	6	0.585"	1	0°	12	0.131"	1	0°	10	0.50"
2	15°	9	.785"	2	30°	7	1.755"	2	5°	13	0.50"	2	10°	11	1.00"
3	30°	10	1.50"	3	60°	8	2.345"	3	10°	14	0.75"	3	20°	12	1.50"
4	45°	11	3.00"	4	75°			4	20°	15	1.00"	4	30°	13	2.00"
5	60°	12	6.00"	5	90°			5	30°	16	1.50"	5	45°	14	2.50"
6	75°	13	7.50"					6	45°	17	2.00"	6	60°		
7	90°	14	8.50"					7	60°	18	3.00"	7	70°		
								8	70°	19	4.00"	8	80°		
								9	80°	20	5.00"	9	90°		
								10	85°	21	6.00"				
								11	90°	22	7.00"				
										23	7.50"				
										24	8.00"				
										25	8.50"				

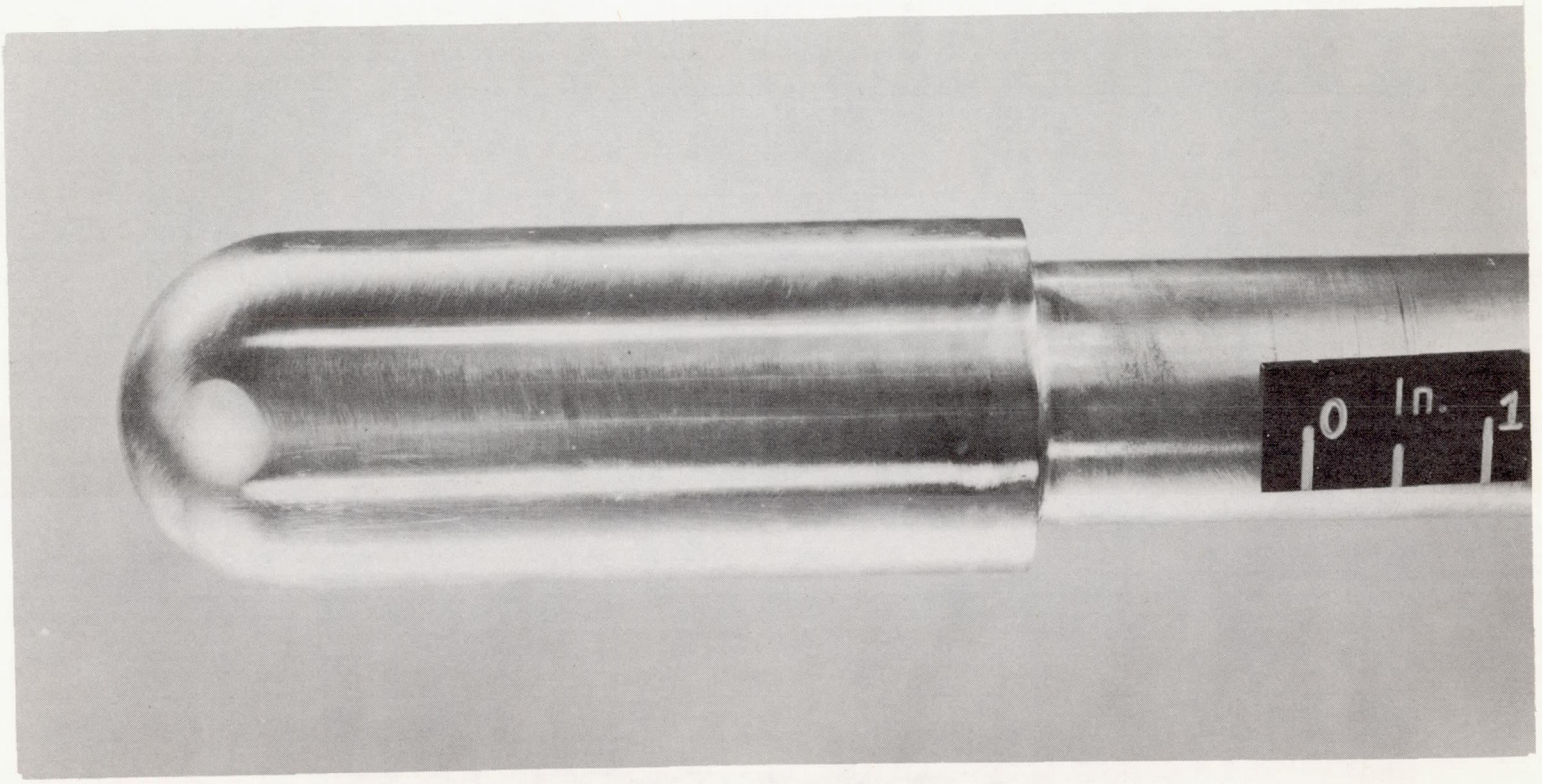
Figure 1.- Typical construction of models.



L-89504

(a) Heat-transfer and pressure models.

Figure 2.- Hemisphere-cylinder models.



L-89994

(b) Recovery-temperature model with 2-inch diameter and 0.005-inch-thick wall.

Figure 2.- Concluded.

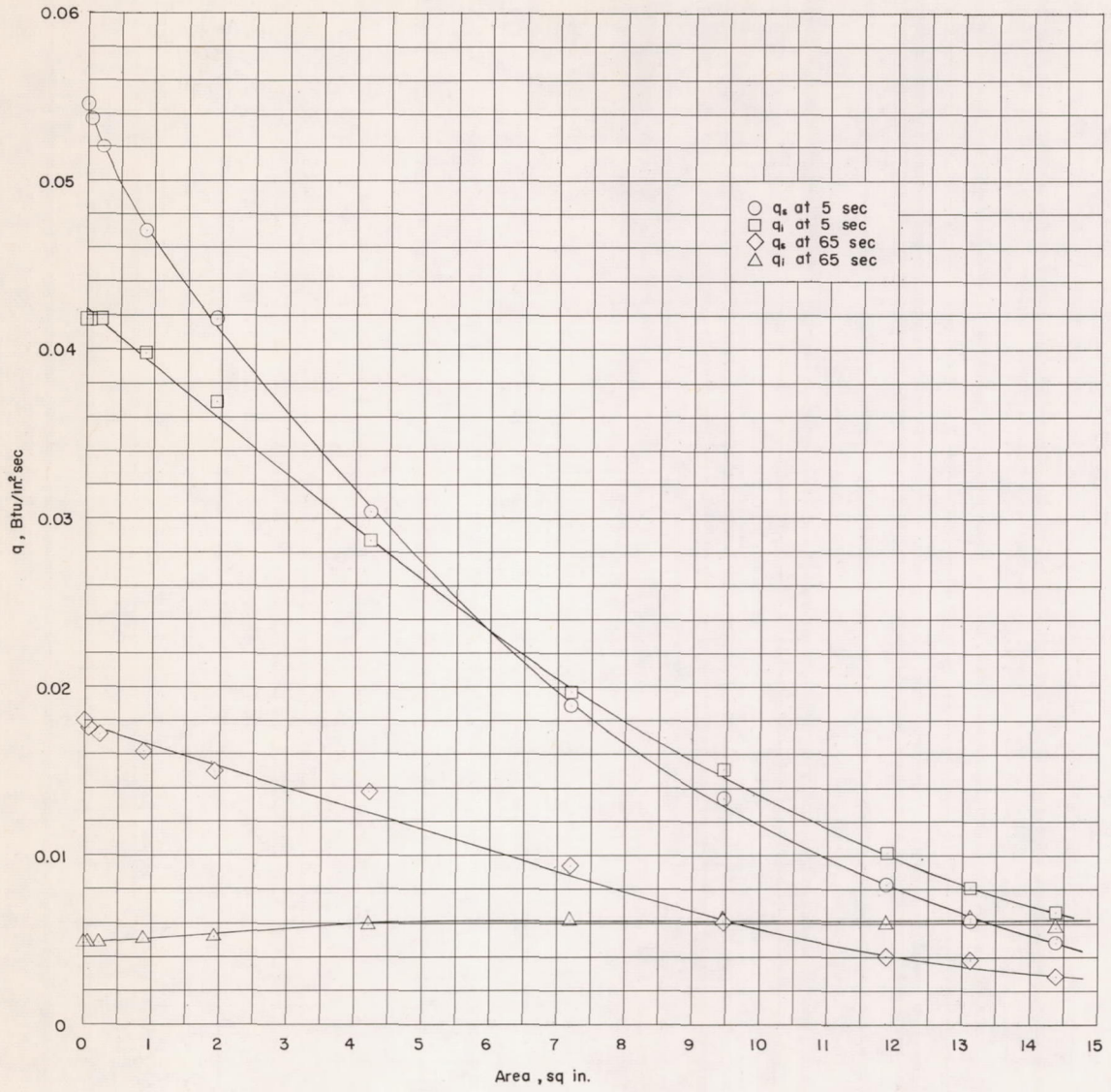


Figure 3.- Heat transfer to the hemisphere of the 3.025-inch-diameter heat-transfer model both with and without the conduction correction.

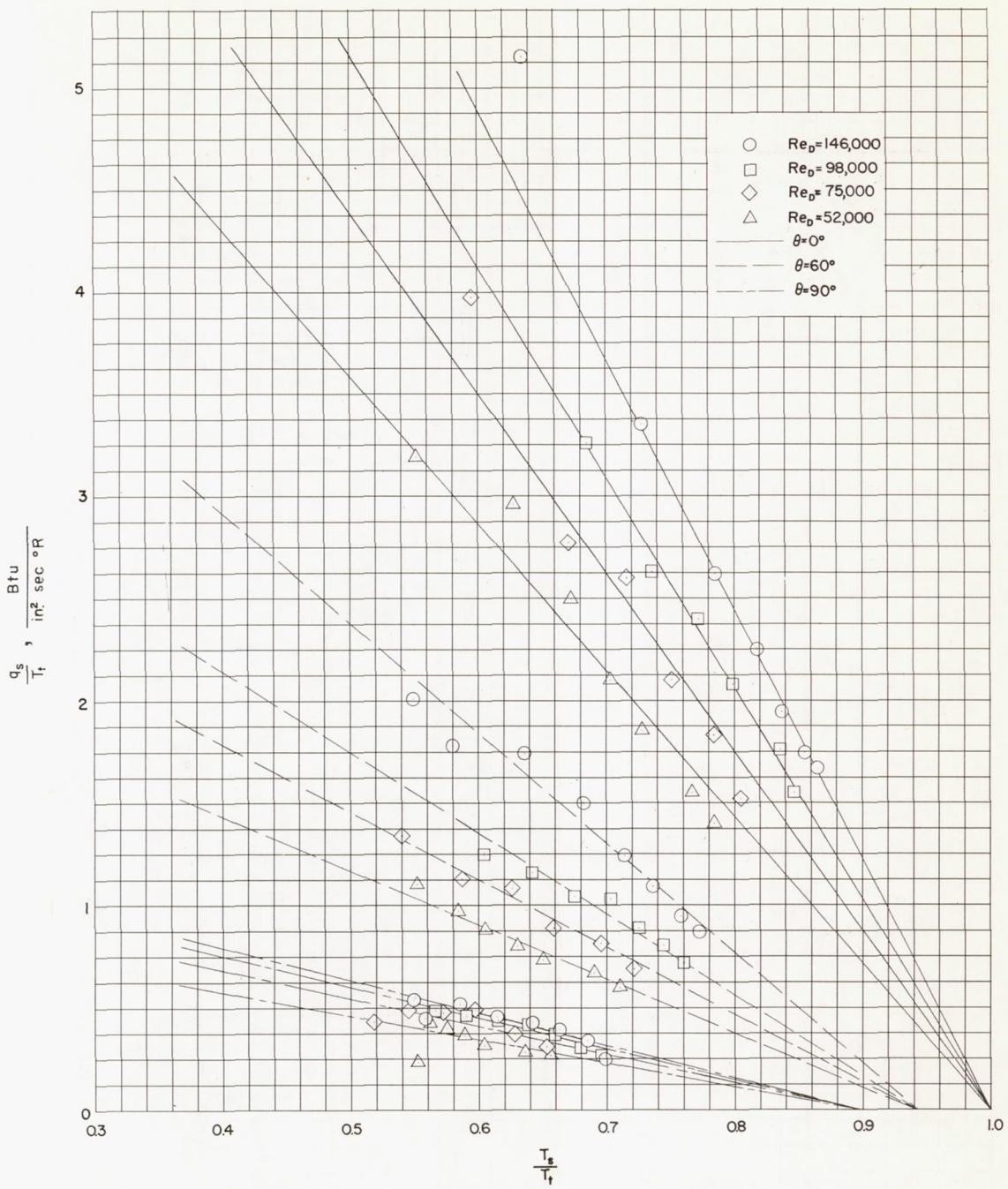


Figure 4.- Heat-transfer rate plotted against surface temperature for various angles of θ on the 3.025-inch-diameter heat-transfer model.

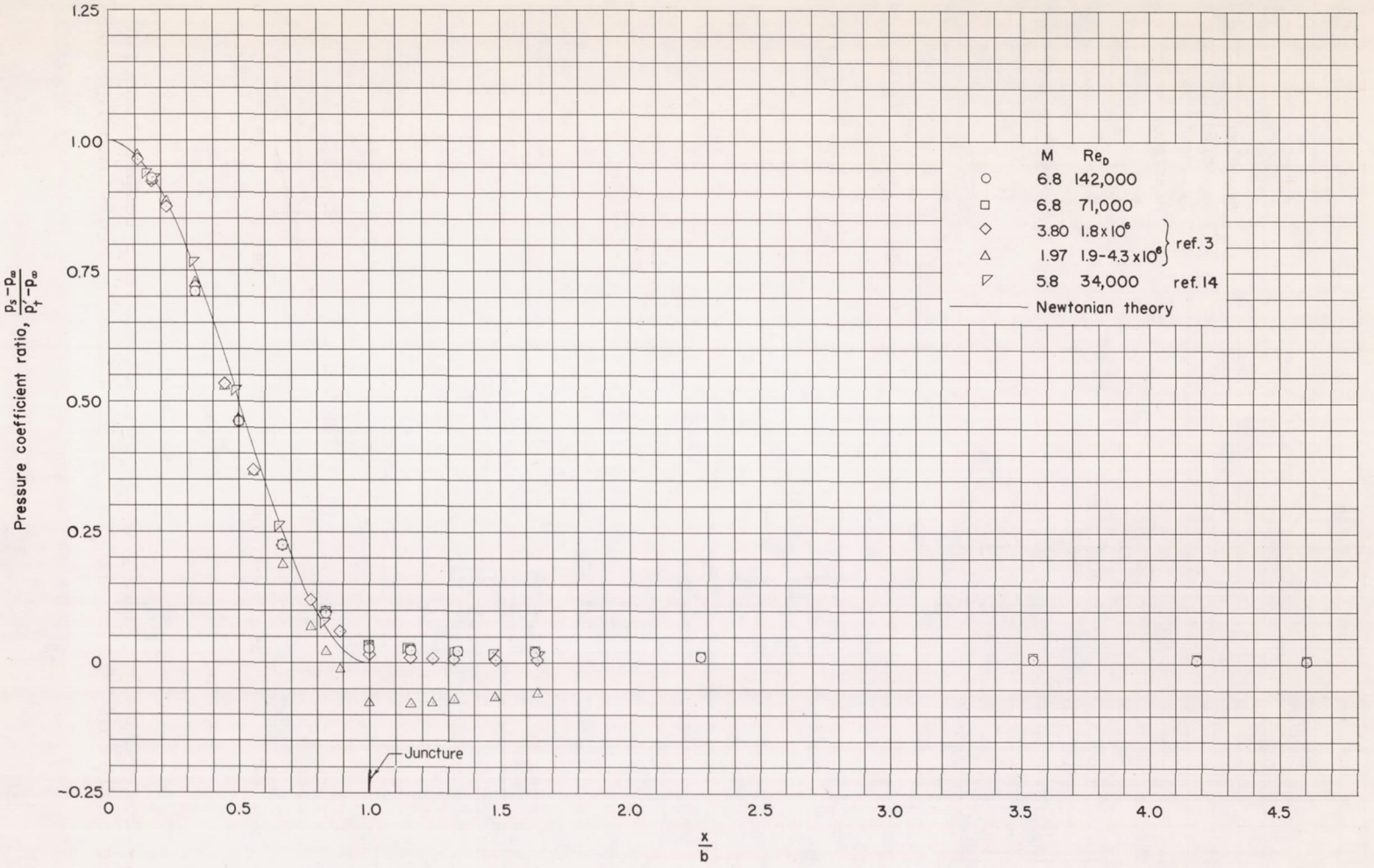


Figure 5.- Longitudinal pressure-coefficient distribution.

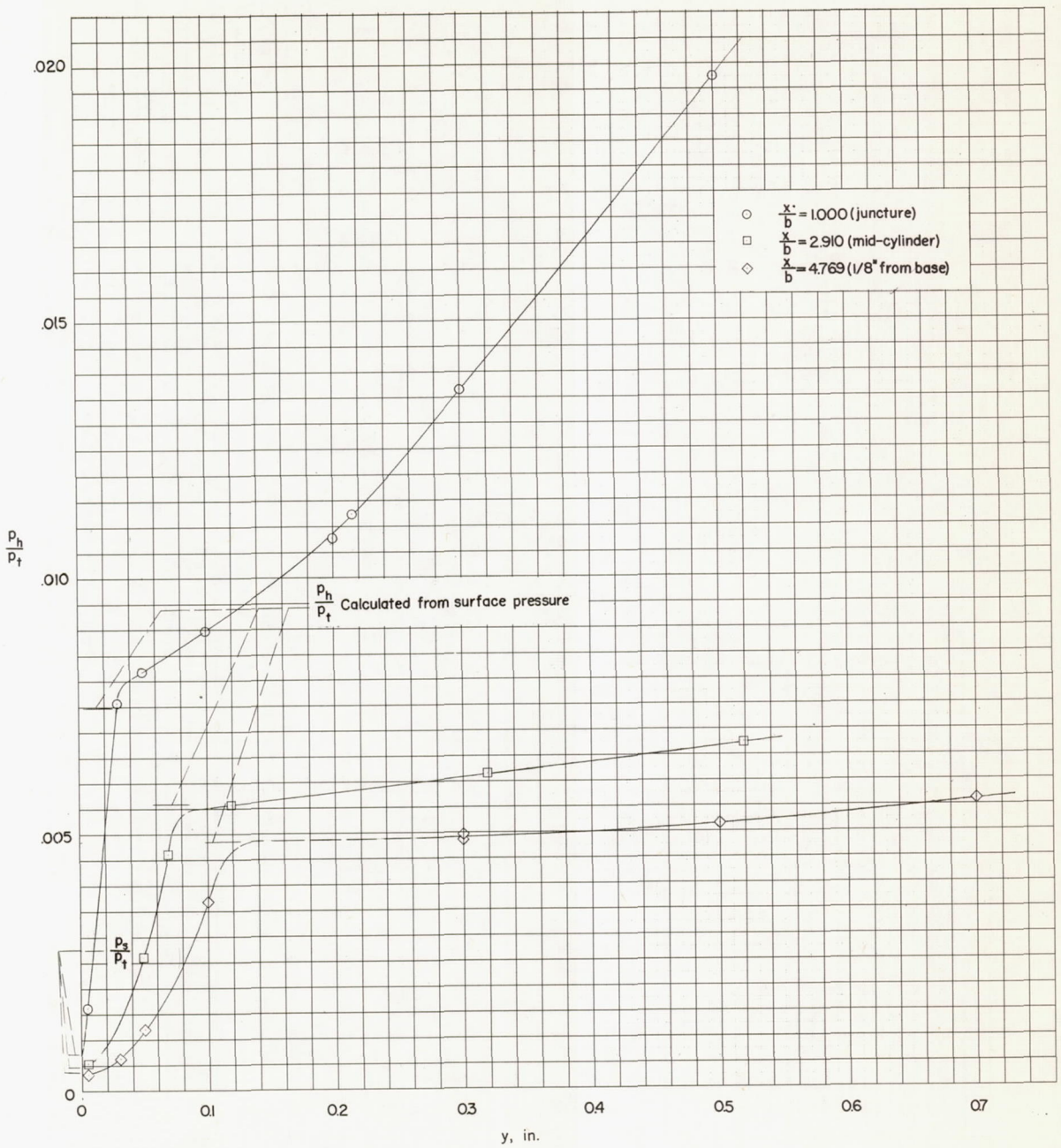


Figure 6.- Pitot surveys of flow near the surface of the cylinder.

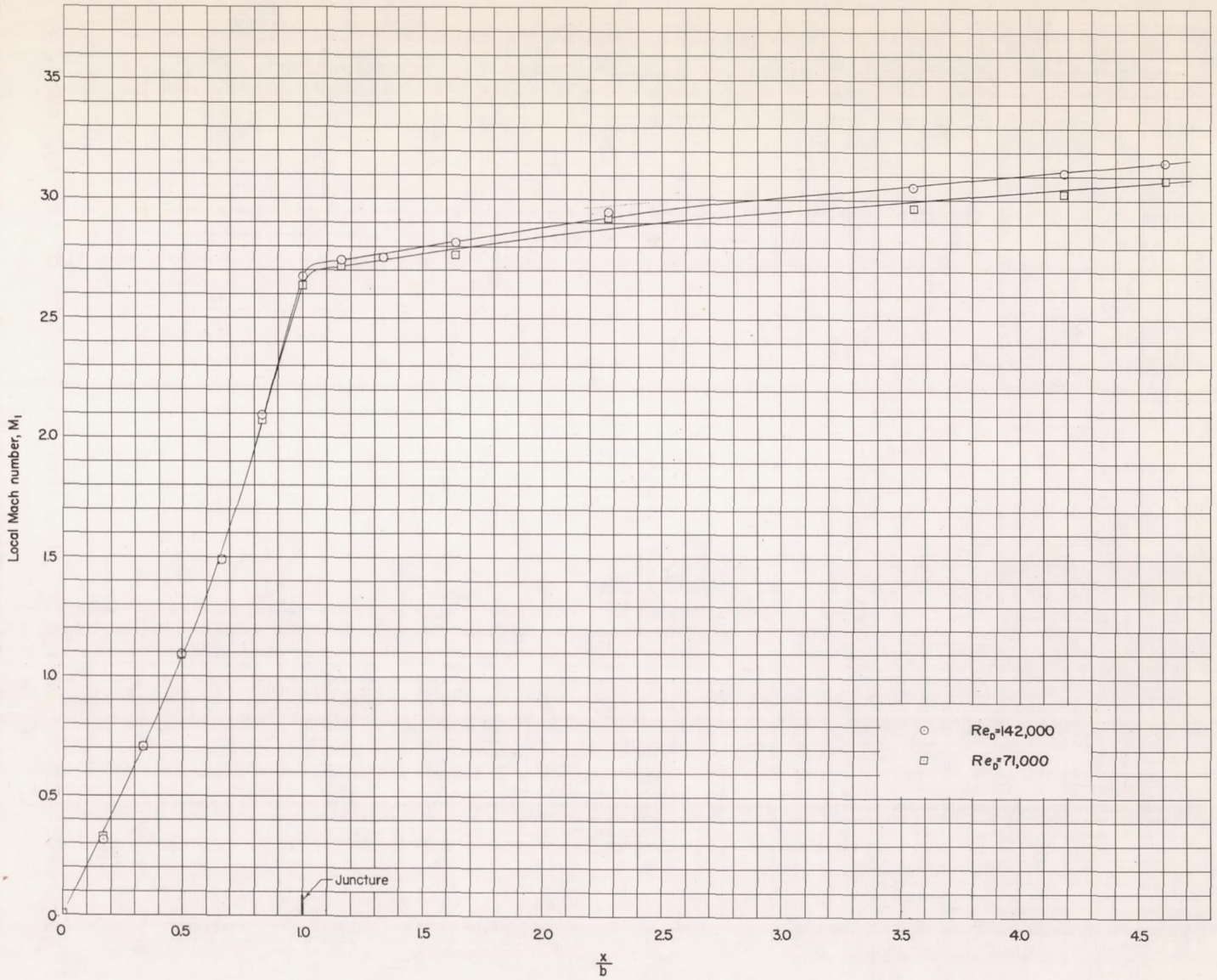


Figure 7.- Variation of local Mach number (outside the boundary layer) along surface.

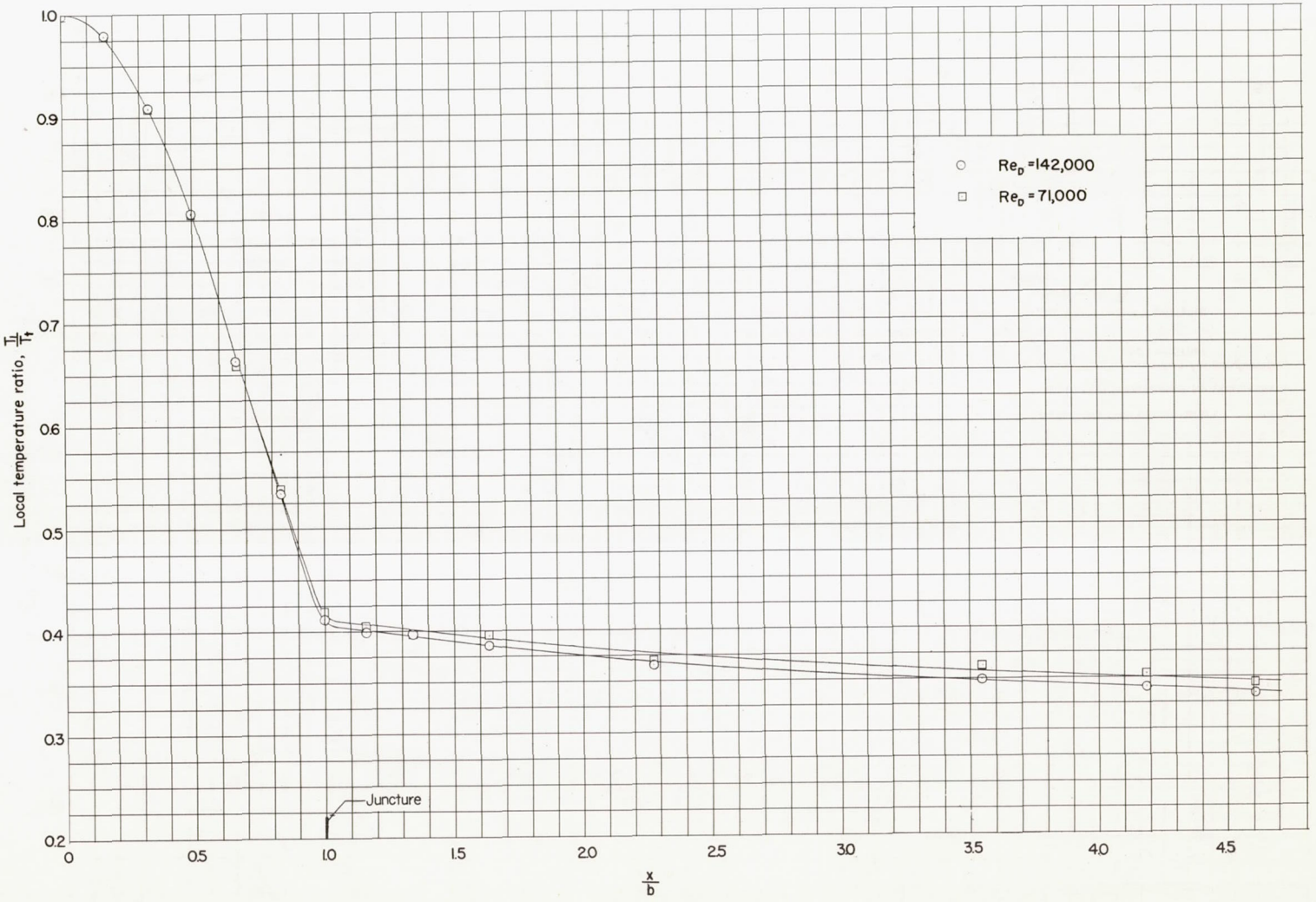


Figure 8.- Variation of the local temperature ratio (outside the boundary layer) along the surface.

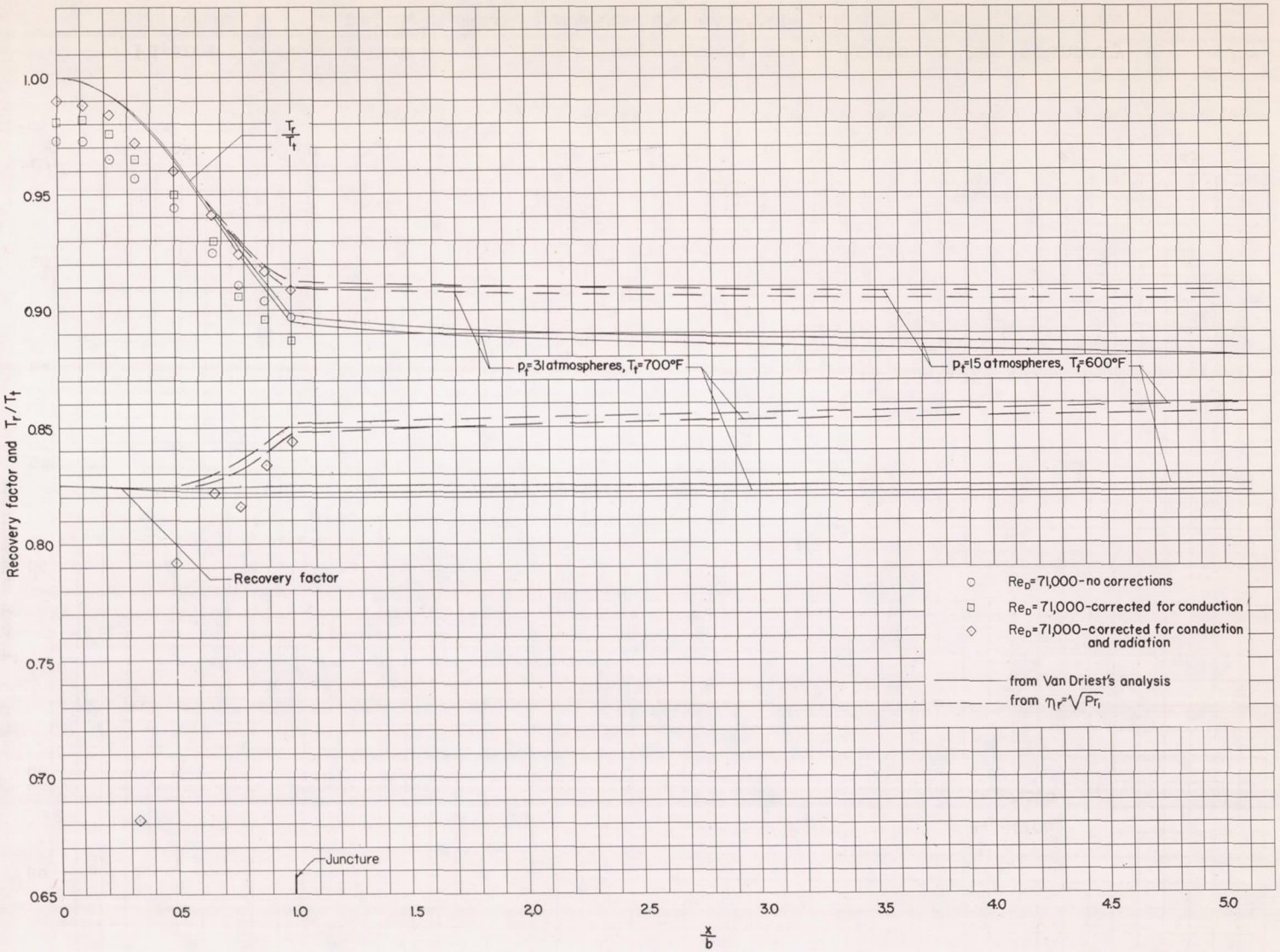


Figure 9.- Variation of the surface temperature ratio and recovery factor along the surface.

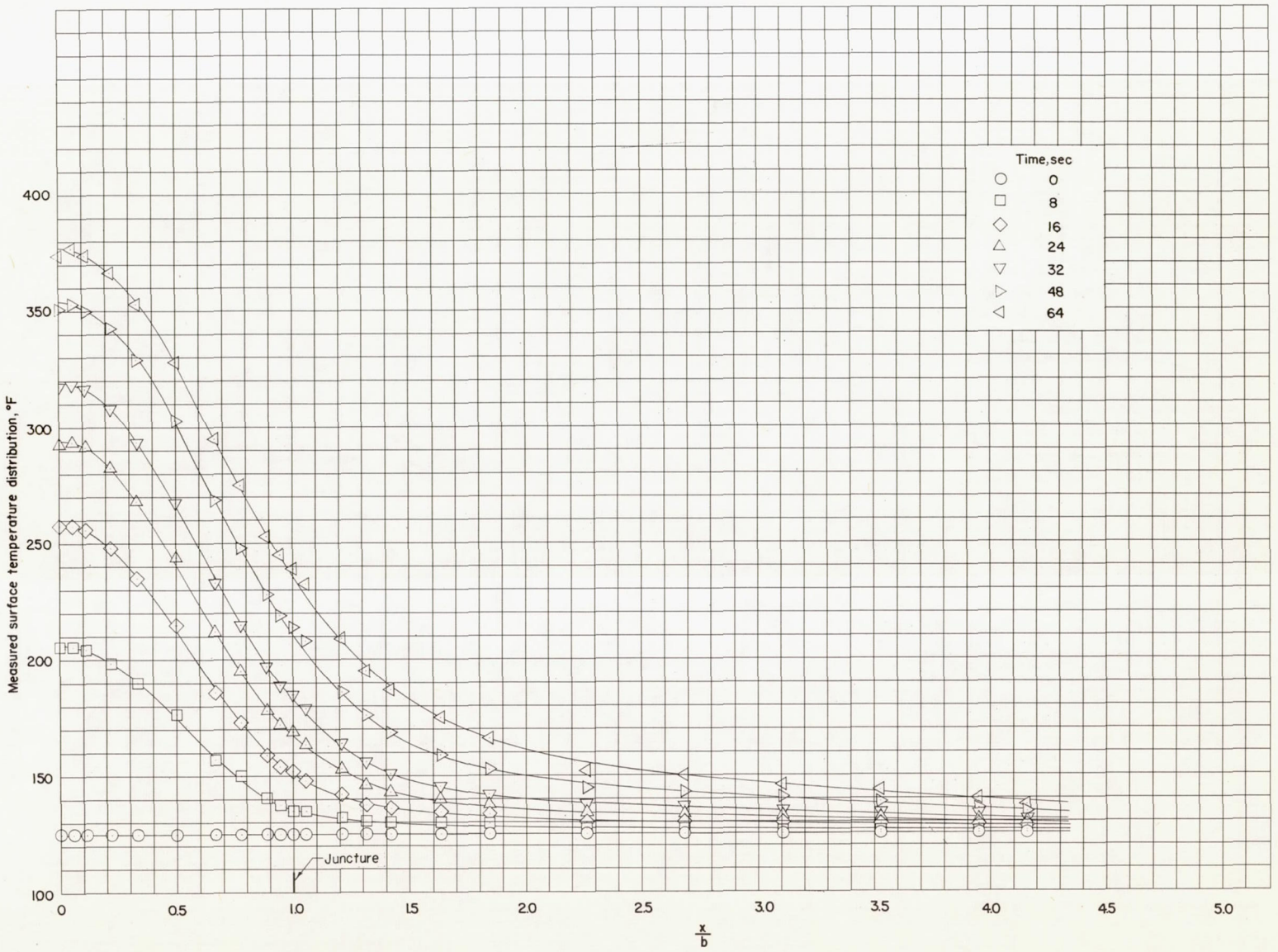


Figure 10.- Typical surface temperature distribution on 3.025-inch-diameter heat-transfer model at various times during a run.

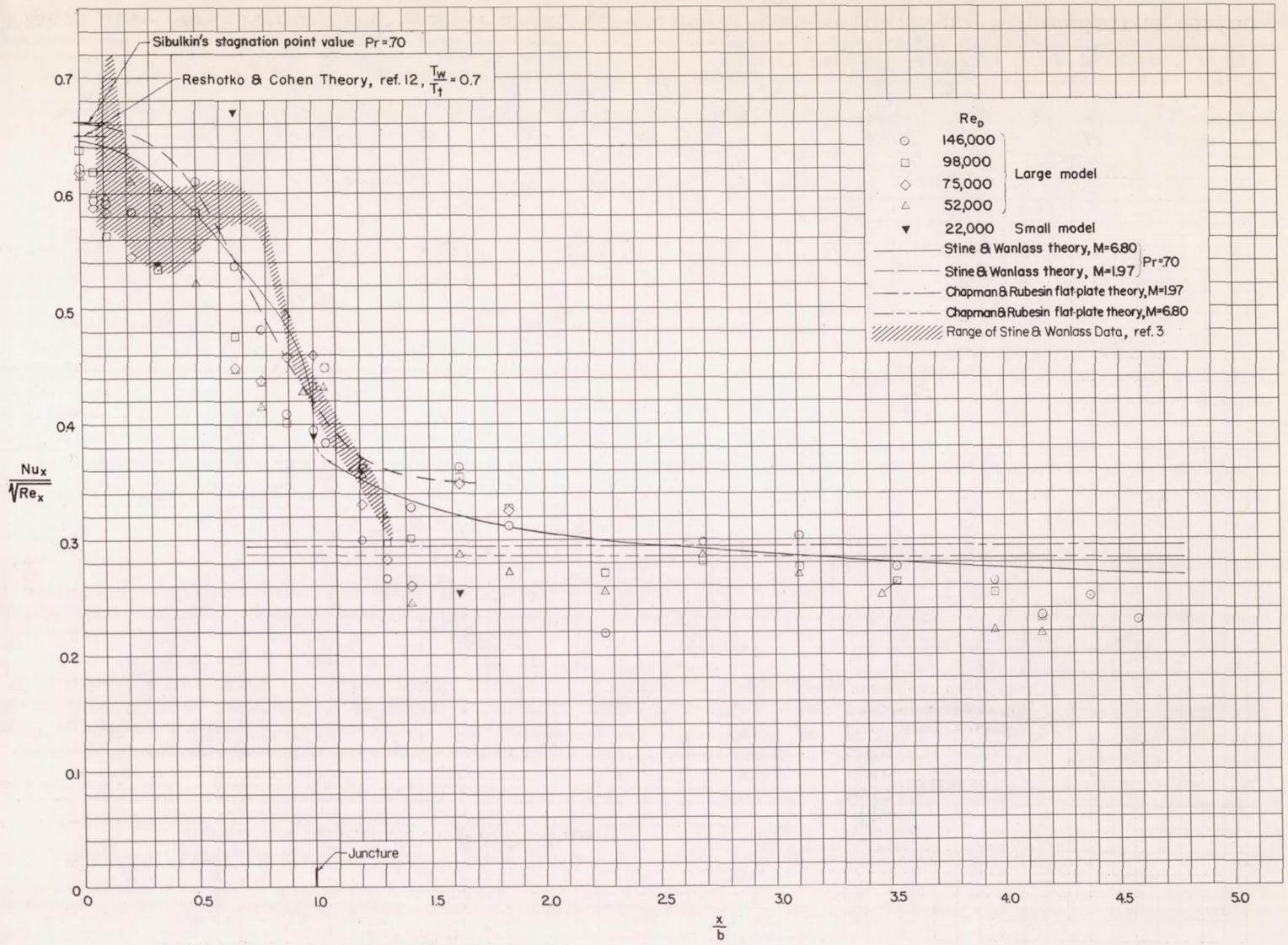


Figure 11.- Variation of the local heat-transfer parameter along the surface.

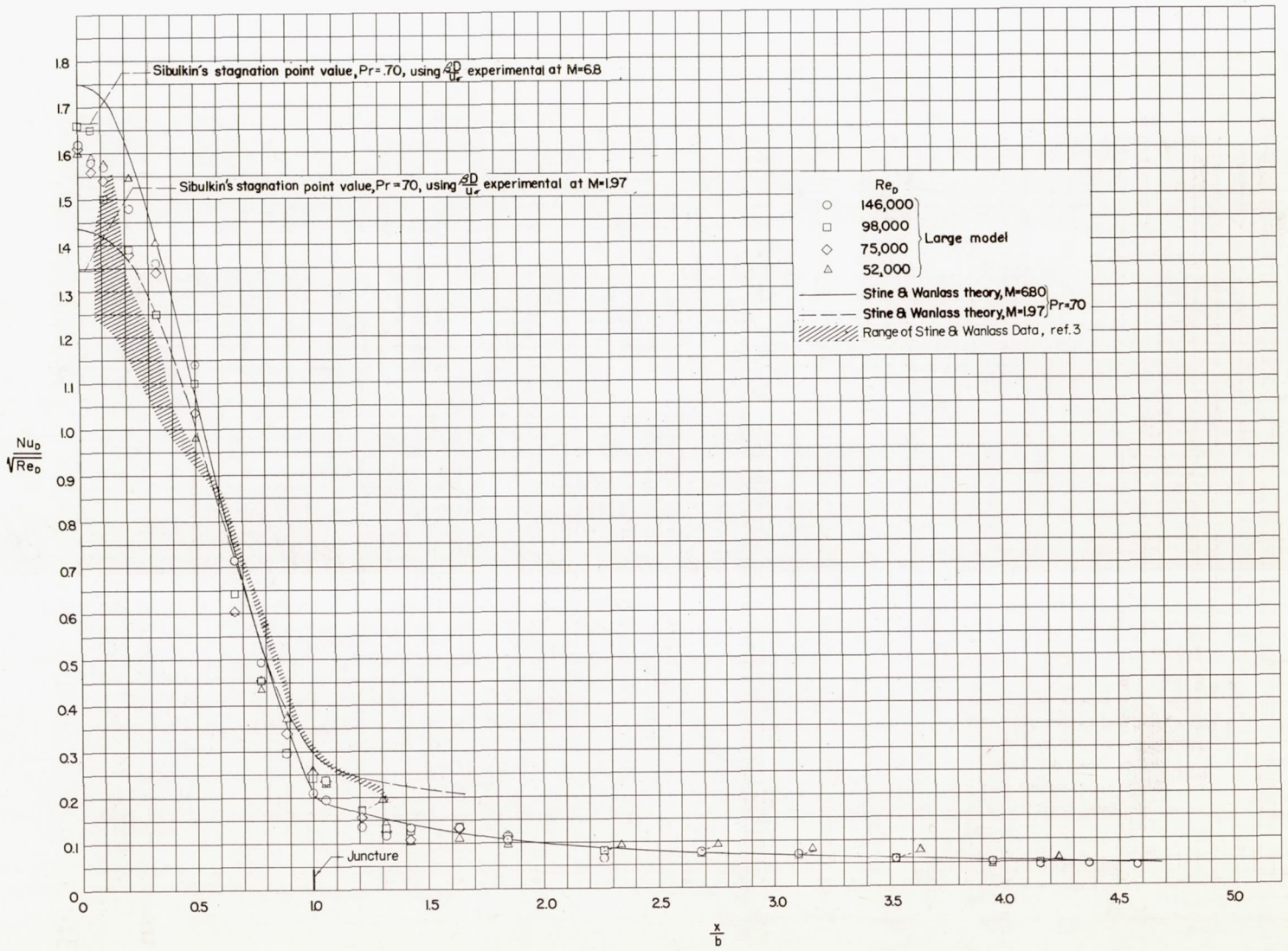
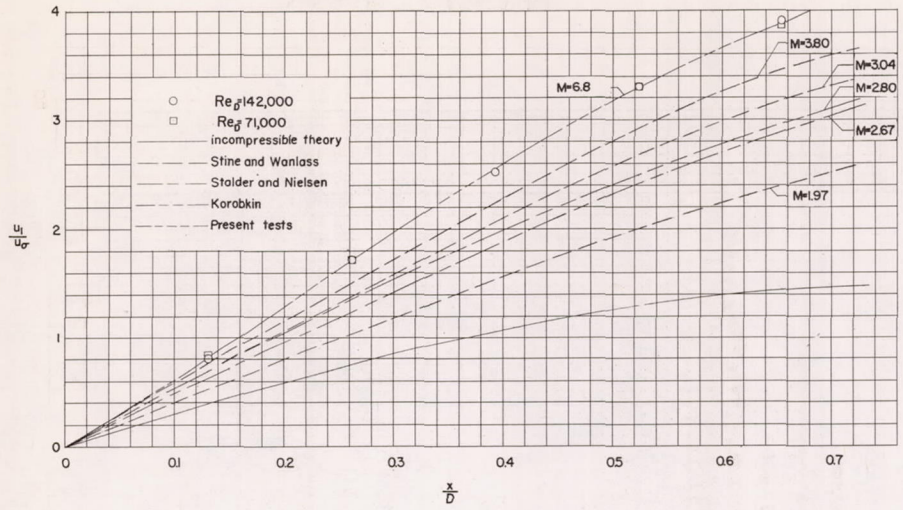
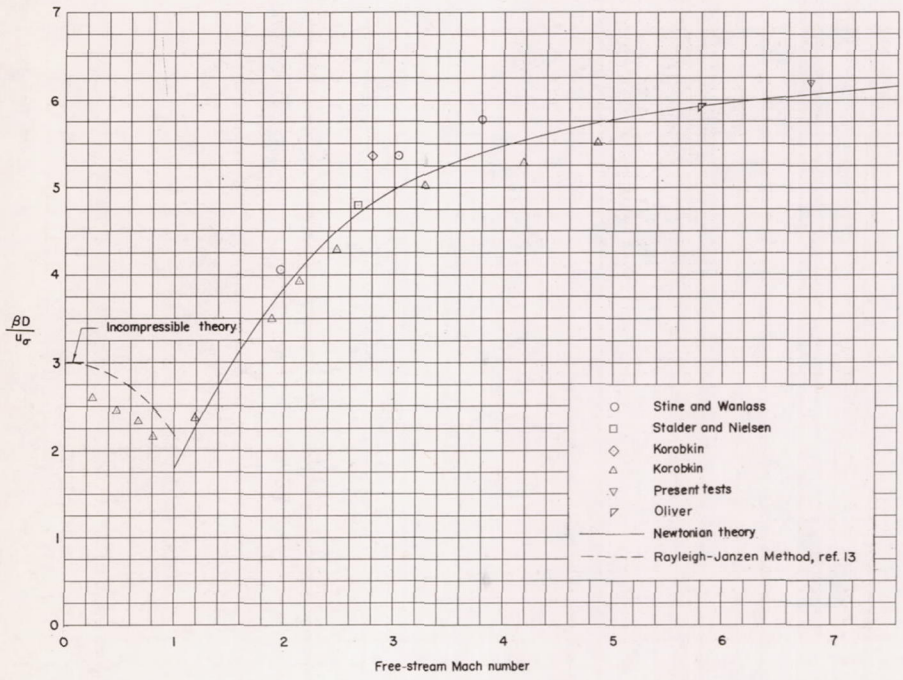


Figure 12.- Variation of the heat-transfer parameter (based on diameter and conditions behind the normal shock) along the surface.



(a) Nondimensional local flow velocity along the surface.



(b) Nondimensional velocity gradient at the stagnation point of the hemisphere plotted against free-stream Mach number.

Figure 13.- Nondimensional flow parameter on the hemisphere outside the boundary layer.

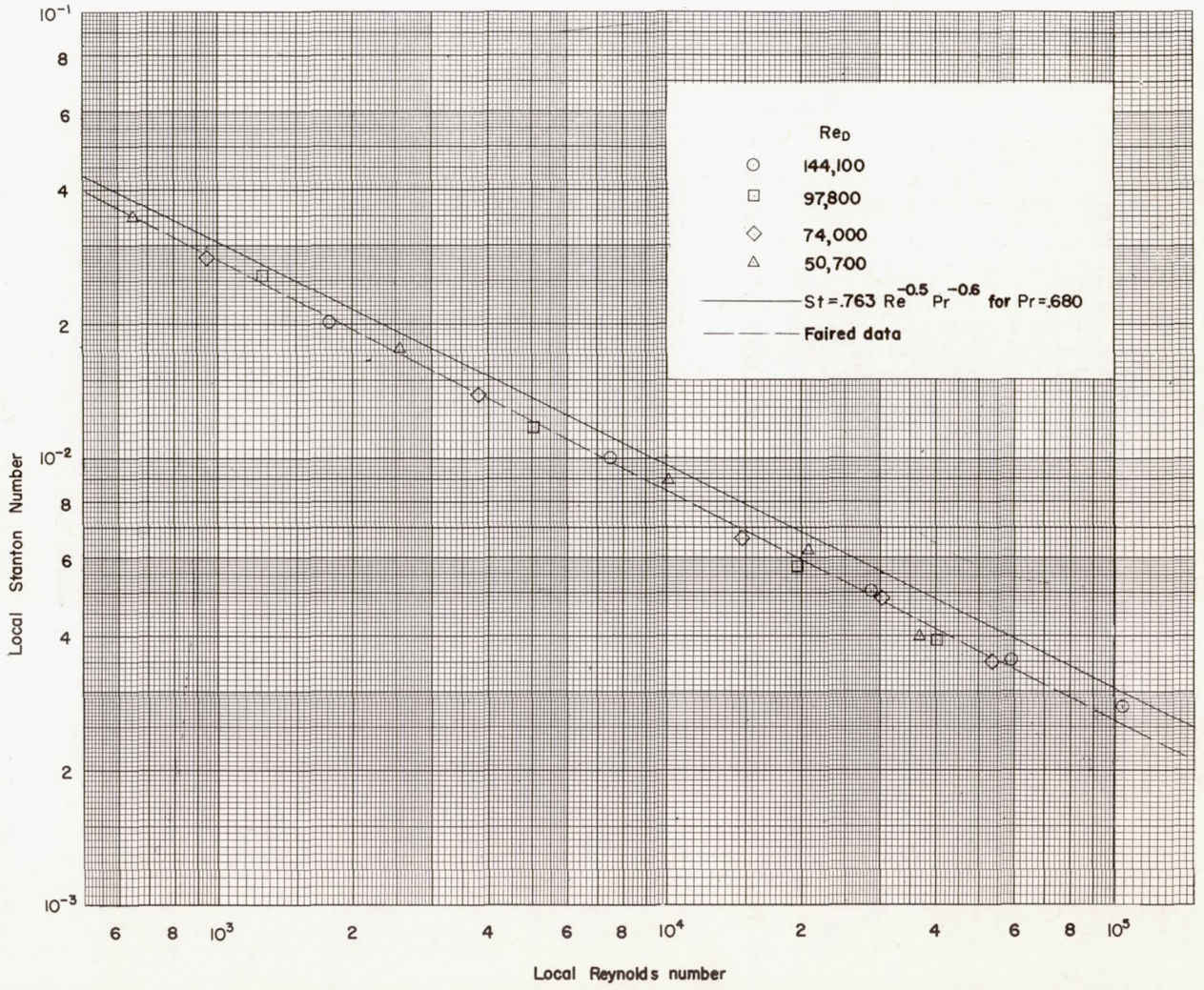


Figure 14.- Variation of the local Stanton number with the local Reynolds number for values of θ from 0° to 45°.

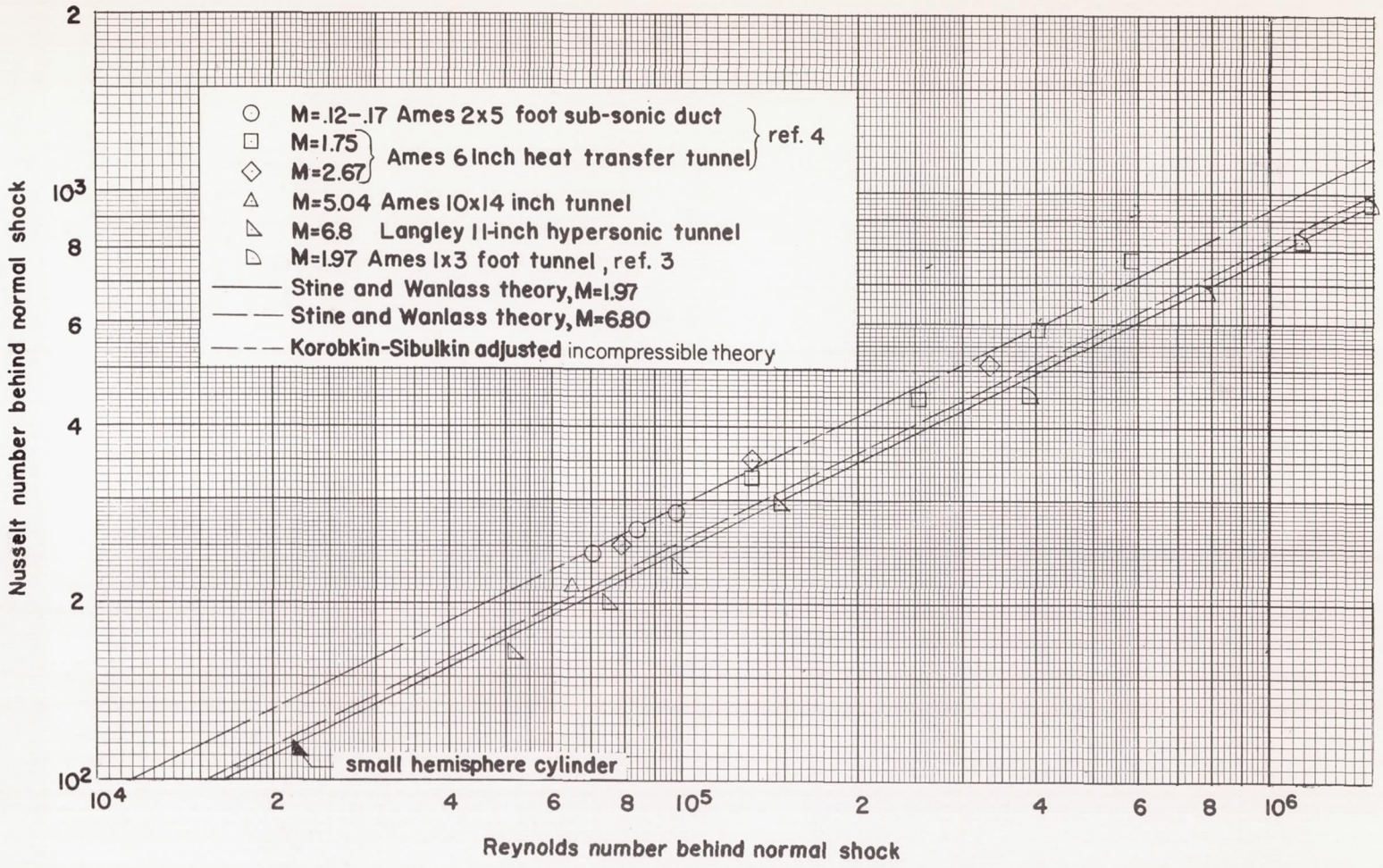
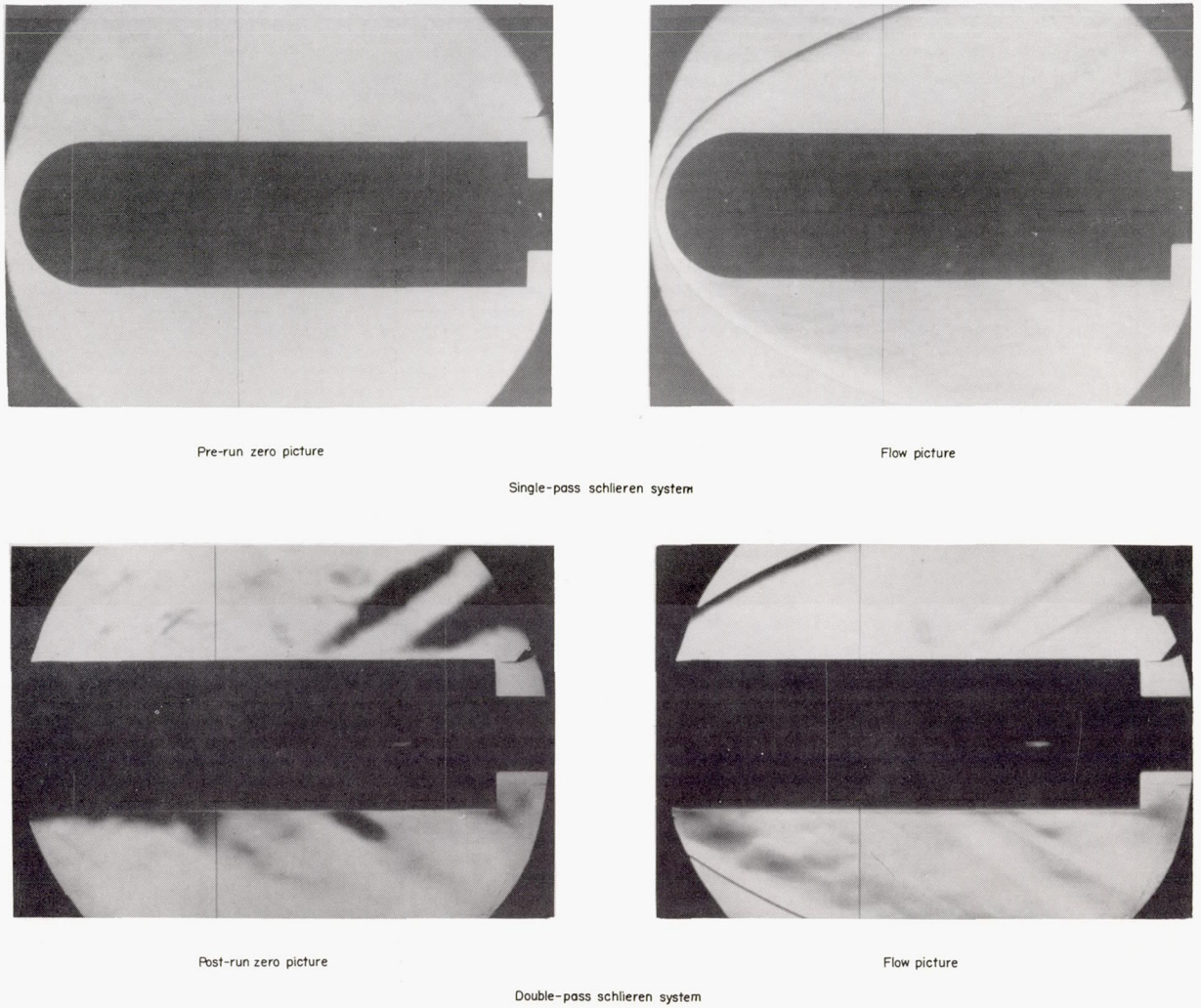


Figure 15.- Average heat transfer on the hemisphere plotted against Reynolds number for conditions behind a normal shock.



L-92450

Figure 16.- Schlieren photographs of shock and boundary layer on hemisphere-cylinder at M = 6.8.

NACA - Langley Field, Va.